Normal State ^{17}O NMR Studies of Sr_2RuO_4 under Uniaxial Stress

Yongkang Luo,[1,2,*] A. Pustogow,[1,‡] P. Guzman,[1] A. P. Dioguardi,[3] S. M. Thomas,[3] F. Ronning,[3] N. Kikugawa,[4] D. A. Sokolov,[5] F. Jerzembeck,[5] A. P. Mackenzie,[5,6] C. W. Hicks,[5] E. D. Bauer,[3] I. I. Mazin,[7] and S. E. Brown[1,†]

[1]*Department of Physics & Astronomy, University of California, Los Angeles, Los Angeles, California 90095, USA*
[2]*Wuhan National High Magnetic Field Center and School of Physics, Huazhong University of Science and Technology, Wuhan 430074, China*
[3]*Los Alamos National Laboratory, Los Alamos, New Mexico 87545, USA*
[4]*National Institute for Materials Science, Tsukuba 305-0003, Japan*
[5]*Max Planck Institute for Chemical Physics of Solids, Dresden 01187, Germany*
[6]*Scottish Universities Physics Alliance, School of Physics and Astronomy, University of St. Andrews, North Haugh, St. Andrews KY16 9SS, United Kingdom*
[7]*Code 6393, Naval Research Laboratory, Washington, D.C. 20375, USA*

(Received 23 September 2018; revised manuscript received 1 February 2019; published 31 May 2019)

The effects of uniaxial compressive stress on the normal state ^{17}O nuclear-magnetic-resonance properties of the unconventional superconductor Sr_2RuO_4 are reported. The paramagnetic shifts of both planar and apical oxygen sites show pronounced anomalies near the nominal **a**-axis strain $\varepsilon_{aa} \equiv \varepsilon_v$ that maximizes the superconducting transition temperature T_c. The spin susceptibility weakly increases on lowering the temperature below $T \simeq 10$ K, consistent with an enhanced density of states associated with passing the Fermi energy through a van Hove singularity. Although such a Lifshitz transition occurs in the γ band formed by the Ru d_{xy} states hybridized with in-plane O p_π orbitals, the large Hund's coupling renormalizes the uniform spin susceptibility, which, in turn, affects the hyperfine fields of all nuclei. We estimate this "Stoner" renormalization S by combining the data with first-principles calculations and conclude that this is an important part of the strain effect, with implications for superconductivity.

DOI: 10.1103/PhysRevX.9.021044

Subject Areas: Condensed Matter Physics, Strongly Correlated Materials, Superconductivity

I. INTRODUCTION

The physics of the unconventional superconductivity (SC) of Sr_2RuO_4 [1] remains a subject of longstanding importance, with particular focus on order-parameter symmetry [2]. There are numerous experimental results consistent with a chiral p-wave superconducting state [3–6], including evidence for time-reversal symmetry breaking for $T < T_c$ [7,8] and lack of suppression of the in-plane spin susceptibility on cooling through the superconducting critical temperature T_c, as deduced from nuclear-magnetic-resonance (NMR) spectroscopy [9,10] and neutron scattering [11]. At the same time, there are other experimental results inconsistent with that interpretation [12–16], and the out-of-plane spin susceptibility also remains constant [10], in contradiction with the expectations for the chiral state [5,17].

For several reasons, the normal state physics of Sr_2RuO_4 is equally topical. It was anticipated at a very early stage that electron-electron interactions are controlled by the Hund's rule coupling [18], and it was later shown within the dynamical mean-field theory that the electrons are subject to strong Hund's rule correlations, while the system remains metallic and far from the Mott insulator regime [19,20]. Mean-field density-functional theory (DFT) calculations within the generalized-gradient approximation are unstable against ferromagnetism [17]. Even though strong correlations lead to fluctuations suppressing this instability, there still remains a substantial Stoner renormalization of the uniform spin susceptibility. This led to the analogy with the triplet superfluidity of ^3He [21] anticipated earlier on the grounds that a related compound $SrRuO_3$

*mpzslyk@gmail.com
†brown@physics.ucla.edu
‡Present address: IFW Dresden, Institute for Solid State Research, P.O. Box 270116, D-01171 Dresden, Germany.

is ferromagnetic [2]. Although later it was found that the leading magnetic instability is at a nonzero momentum $\mathbf{q_0} \approx (\pm 0.6, \pm 0.6, 0)\pi/a$ [22,23], the proximity to a ferromagnetic state dominates the debate related to the superconducting order-parameter symmetry [6,24].

An additional feature is the proximity to a 2D Lifshitz point [25] associated with a van Hove singularity (VHS), and the question as to its relationship to both normal state properties and nature of the superconducting state. Recently, striking physical property changes, including a factor of 2.5 increase in superconducting critical temperature T_c from 1.4 to 3.5 K [26] accompanied by a pronounced non-Fermi-liquid behavior of the resistivity [27] were observed under application of in-plane strain ε_{aa}. This was tentatively interpreted as a Fermi-level crossing of the VHS when ε_{aa} reaches a critical value ε_v. Since direct experimental evidence is still lacking, it is important to test this interpretation in complementary studies of the normal state while subject to strain. Also, the VHS is expected to influence quite differently the triplet and singlet superconducting states, and this provides further motivation for physical property studies under strain. For singlet pairing, the order parameter (SC gap) can be large at the VHS (e.g., for the $d_{x^2-y^2}$ symmetry), and thus, the local density-of-states (DOS) enhancement at the VHS is very beneficial. On the contrary, the triplet order parameter at precisely the Lifshitz point is zero by symmetry, and therefore, a triplet state is less suited to take advantage of the VHS unless the pairing interaction itself is enhanced. Since the DOS enhancement brings the system closer to ferromagnetism, the latter case is possible [28].

With these issues in mind, we set out to verify experimentally that the same strain at which T_c peaks indeed corresponds to a maximum in the DOS and to assess as quantitatively as possible the change in the DOS and Stoner enhancements to the susceptibility under strained conditions. To this end, NMR measurements inform us on the details of the normal state through site and orbitally specific hyperfine couplings. Indeed, the enhancement is evident in the results presented, and moreover, the inferred enhancement semiquantitatively accounts for the transport results in Ref. [27]. Looking ahead, it is worth emphasizing that the method is considered a litmus test for the superconducting state parity [9,29], including any strain-induced order-parameter changes. The results presented in the next sections are normal state ^{17}O NMR spectroscopy for in-plane $\mathbf{B}\|\mathbf{b}$ and out-of-plane $\mathbf{B}\|\mathbf{c}$ fields, as well as ^{17}O NMR relaxation rates for $\mathbf{B}\|\mathbf{b}$ in the presence of **a**-axis strain ε_{aa}. These results are interpreted by way of complementary DFT calculations.

II. EXPERIMENTAL DETAILS

Single-crystalline Sr_2RuO_4 used for these measurements is grown by the floating-zone method [1]. Smaller pieces are cut and polished along crystallographic axes with typical dimensions $3 \times 0.3 \times 0.15$ mm^3 and with the longest dimension aligned with the **a** axis. ^{17}O isotope ($^{17}I = 5/2$, gyromagnetic ratio $^{17}\gamma = -5.7719$ MHz/T [30]) spin labeling is achieved by annealing in 50% ^{17}O-enriched oxygen atmosphere at 1050 °C for two weeks [9,31]. The sample quality is not observably changed following this procedure, with $T_c \approx 1.44$ K identified by specific heat measurements (see the Supplemental Material [32]). For the NMR experiments, the sample is mounted on a piezoelectric strain cell (Razorbill, UK) with an effective (exposed) length $L_0 \sim 1$ mm [see Fig. S1(a) in the Supplemental Material [32]). Three samples (labeled as *S*1, *S*2, and *S*3) are measured in this work. A nominal compressive stress is applied along the **a** axis, with corresponding strains ($\varepsilon_{aa} \equiv \delta L/L_0$) estimated to be up to approximately 0.72% using a precalibrated capacitive dilatometer; The accuracy is limited by the unknown deformations of the epoxy clamp [33]. For reference, the observed maximum $T_c(\varepsilon_{aa})$ occurs at a quantitatively similar displacement as reported in Ref. [26], $T_c^{\max} = T_c(\varepsilon_v)$, with $\varepsilon_v \simeq -0.6\%$. Most of the NMR measurements are performed at fixed temperature $T = 4.30(5)$ K and carrier frequency $f_0 = 46.8$ MHz ($B \simeq 8.1$ T) using a standard Hahn echo sequence. Spectra including satellite transitions are collected in field-sweep mode, whereas a close examination of the central transition ($-1/2 \leftrightarrow 1/2$) for both in-plane and apical sites is carried out under fixed-field conditions. Some field and temperature dependence is explored, too. The application of NMR in conjunction with the piezoelectric driven *in situ* strain is particularly challenging because of the severe constraints on sample size. As a result, some modifications to standard resonant tank circuit configurations are adopted.

For insight into the strain-induced changes to the NMR shifts, and particularly those associated with the VHS, density-functional calculations using the linear augmented-plane-wave package WIEN2K [35] are performed, including spin-orbit interaction. The specific objective is to extract at least semiquantitative information about the origin, evolution, and relative importance of the various individual contributions to the net Knight shifts. A local density approximation for the exchange-correlation functional, a k-point mesh of $41 \times 41 \times 41$, and the expansion parameter $RK_{\max} = 7$ are utilized. Further, the optimized structures of Ref. [26] are used and then interpolated to assure that the strain at which the VHS crosses the Fermi level is included. It turns out that the proximity to a (ferromagnetic) quantum critical point forces some adjustments to the standard procedure. One reason lies with the mean-field approach: DFT overestimates the tendency to magnetism, because in reality, the Hund's rule derived interaction I and, correspondingly, the Stoner renormalization S, are reduced by quantum fluctuations that are not accounted for. A second challenge originates with the very narrow calculated DOS singularity at the VHS: In relation to the Knight-shift evaluation, an external magnetic field

is applied followed by the computation of generated hyperfine fields. The singularity full width at half maximum is approximately 3 meV and holds only 0.0015 e^- in each spin channel. As a result, an external field producing sufficiently strong hyperfine fields (compared to the computational noise), is too large to properly monitor the VHS peak. Nevertheless, the calculations at the larger fields produce useful information, in part because the origin of the net Knight shifts in terms of individual contributions is obtained.

III. RESULTS AND DISCUSSION

The geometry of our experiment is depicted in Fig. 1(a) [36]. Each Ru ion is coordinated octahedrally by four planar O(1) and two apical O(2) oxygen sites, with a small elongation along the **c** axis. While **a**-axis strain ε_{aa} renders the sites O(1) and O(1′) crystallographically inequivalent, their local symmetries are different even for the unstrained case and external field **B**‖**b**. The field-sweep spectra in Fig. S2 in the Supplemental Material [32] are described by parameters (shifts, electric field gradient) similar to previous reports for ^{17}O NMR in unstrained Sr_2RuO_4 [29,36], with five NMR transitions for each of three (two) distinct sites for **B**‖**b** (**B**‖**c**) [32].

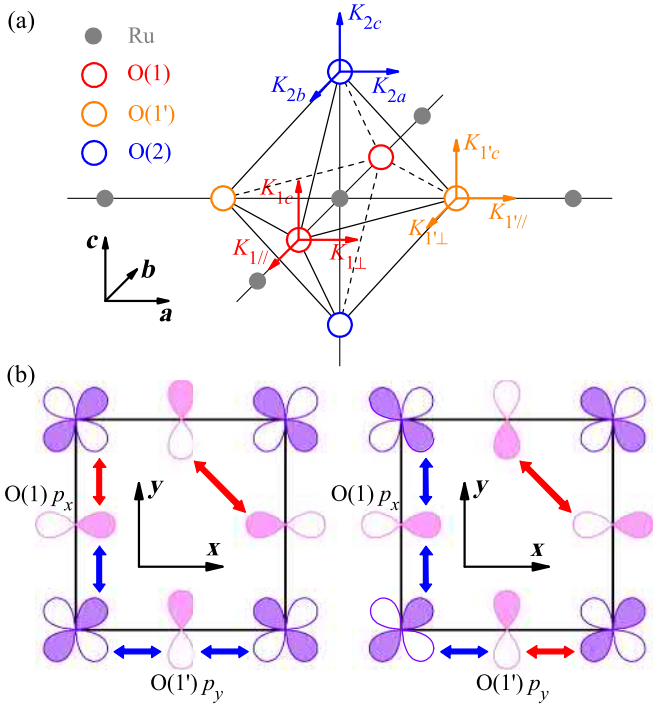

FIG. 1. (a) Configurations of planar O(1) and O(1′) in the RuO_2 plane and apical O(2) in the SrO layer around Ru ion in a unit cell of Sr_2RuO_4. Compressive strain is applied along the **a** axis (ε_{aa}); magnetic fields are applied orthogonal, ‖**b**, ‖**c**. Arrows signify the principal axes of Knight-shift tensors. (b) Orbitals forming the γ band at the X (left) and Y (right) points in the Brillouin zone. The blue (red) double arrows show positive (negative) signs of orbital overlaps. Note that at the Y point, only O(1)p_x orbitals participate in the band formation, while O(1′)p_y suffers from cancellation of the left and right overlaps. The weak O(1)-O(1′) overlaps also cancel out, as shown in the figure.

The most relevant orbitals for the ^{17}O couplings are Ru 4d t_{2g}, which hybridize with O p states to form the quasi-2D γ band, predominantly from the d_{xy} orbital, and similarly, the quasi-1D α and β bands from the $d_{zx,yz}$ orbitals, Fig. 1(b). The spin-orbit coupling (SOC) mixes these bands. While mixing is strongest along the Brillouin zone diagonal [Γ-M in momentum space; see Fig. 2(b)] [37,38], it is more important here that it mixes the d_{xy} and d_{yz} bands at Y. The latter has the effect of pushing down the lower band (d_{xy}) by about 20 meV, which shifts the critical strain ε_v where the Lifshitz transition shows up in the calculations from about 1.0% to about −0.85%. Additional mass renormalization not accounted for in the DFT calculations reduces the critical strain still further, consistent with the experimentally observed maximum in T_c between −0.55% and −0.60% [26,32].

^{17}O NMR spectra under varying strain conditions are shown in Fig. 3. The two panels depict the central transition for all three sites O(1), O(1′), and O(2) measured with carrier frequency $f_0 = 46.80$ MHz and magnetic field $B = 8.0970$ T applied parallel to the **b** (left panel) and **c** axes (right panel), respectively. The peaks for O(1), O(1′), and O(2) appear at the labeled frequencies measured relative to f_0. The vertical dashed lines correspond to zero shift. O(2), having relatively minor contribution to the

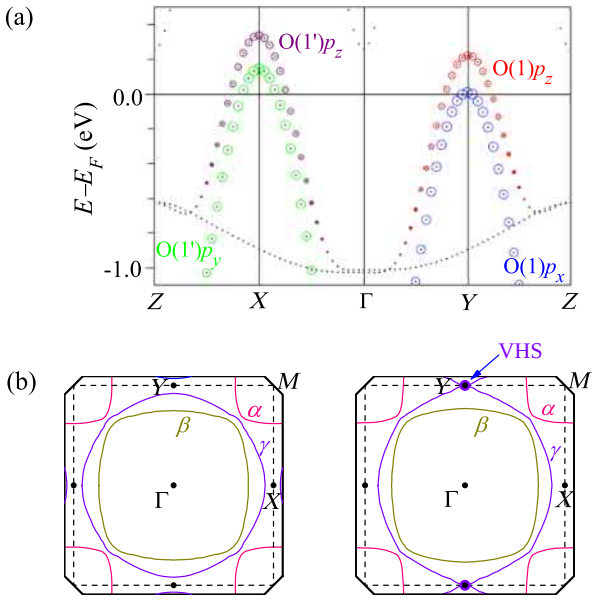

FIG. 2. (a) Bands along the Γ-X and Γ-Y directions. The partial weights of the O(1)p_x, O(1′)p_y, O(1)p_z, and O(1′)p_z orbitals are shown in green, blue, red, and purple, respectively. Other oxygen orbitals have far lesser weight near the Fermi energy. (b) Depictions of the 2D Fermi surfaces, with quasi-2D γ (d_{xy}) and quasi-1D α, β ($d_{zx,yz}$) bands.

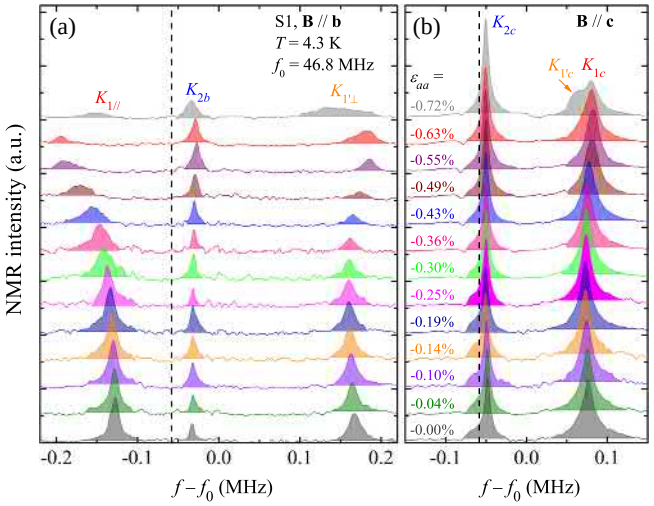

FIG. 3. NMR spectra of the central transitions ($\frac{1}{2} \leftrightarrow -\frac{1}{2}$) of O(1), O(1′), and O(2) at various strains for magnetic field along the **b** (left) and **c** axes (right). The measurements are carried out at fixed temperature ($T = 4.3$ K) and field ($B = 8.0970$ T) and radio frequency $f_0 = 46.80$ MHz. The curves are vertically offset for clarity. The dash vertical line corresponds to $^{17}\gamma = -5.7719$ MHz/T ($D_2^{17}O$) [30] with zero shift.

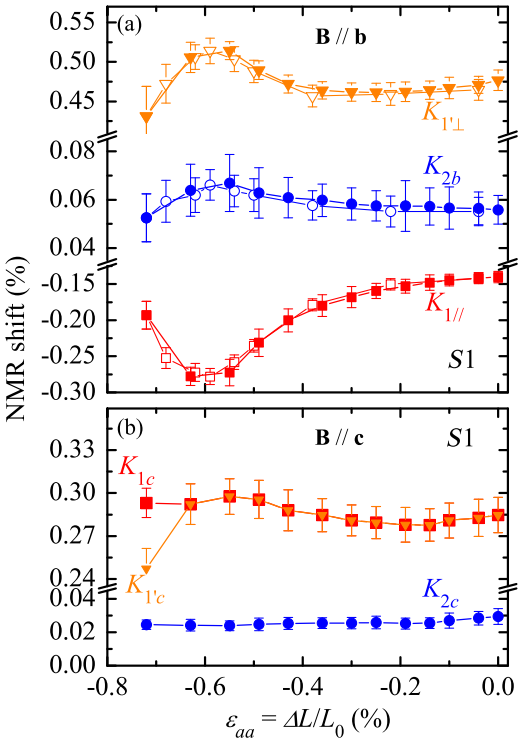

FIG. 4. Measured NMR shifts for $\mathbf{B}\|\mathbf{b}$ (a) and for $\mathbf{B}\|\mathbf{c}$ (b) at $T = 4.3$ K. The solid (open) symbols represent increasing (decreasing) $|\varepsilon_{aa}|$. The error bars are determined by the half-width of the peaks. Similar results are reproduced from several samples; see Fig. S5(a) in the Supplemental Material [32].

Ru bands [there is only a weak coupling of the O(2) $p_{x,y}$ with Ru $d_{zx,yz}$ orbitals, respectively] exhibits a very small Knight shift. In contrast, Knight shifts for O(1) and O(1′) vary strongly and show clear extrema at strain $\varepsilon_{aa} = \varepsilon_v$ corresponding to the putative VHS and defined as where $T_c(\varepsilon_{aa})$ is largest. The anomaly is most pronounced for the in-plane field orientation. For larger strains, there is significant broadening, tentatively attributed to a strong strain dependence of the spin susceptibility combined with a distribution of strains within the sample. (Note that asymmetries in mounting geometry lead naturally to crystal bending.) In the right-hand panel, O(1, 1′) spectral peaks appear indistinguishable at small strain, with pronounced broadening and splitting appearing for strains exceeding ε_v. The NMR shifts K defined as the relative change of resonance frequency referenced to that observed for $D_2^{17}O$ are shown as a function of ε_{aa} in Fig. 4. Similar results reproduced from other samples can be found in Fig. S5(a) of the Supplemental Material [32]. One striking feature is that the Knight-shift anomaly near $\varepsilon_{aa} \approx \varepsilon_v$ is seen in all the measured ^{17}O sites, not only in O(1) that is most relevant to VHS at Y.

In metals, the NMR shift is governed by three main contributions resulting from spin and orbital responses to the applied field: (i) isotropic coupling from the Fermi contact interaction and core polarization, (ii) anisotropic coupling of the dipolar field generated by the electronic spin away from the nucleus, and (iii) fields generated by orbital currents. For computational purposes, this partitioning of the hyperfine field contributions can be summarized as

$$\mathbf{h}(\mathbf{r}) = \mathbf{h}_s + \mathbf{h}_d + \mathbf{h}_o = -\beta\left[\frac{8\pi \mathbf{s}\delta(\mathbf{r})}{3} + \frac{3\mathbf{r}(\mathbf{r}\cdot\mathbf{s}) - r^2\mathbf{s}}{r^5} + \frac{\mathbf{L}}{r^3}\right], \tag{1}$$

where $\mathbf{s}$ is the spin moment of an electron, and $\mathbf{L}$ its orbital moment. Real-space integration results in the total local field. Note that $\mathbf{h}_s$ has no anisotropy, while $\mathbf{h}_d$ gives no isotropic contribution ($\mathbf{h}_o$ has both).

The net spin magnetization is written as

$$M_s = \chi_s H, \tag{2}$$

where the full uniform spin susceptibility χ_s can be expressed using the Stoner factor S,

$$\chi_s = (m^*/m_0) S \chi_{s0}^{\mathrm{DFT}}, \tag{3}$$

where χ_{s0}^{DFT} is the *noninteracting* spin susceptibility proportional to (neglecting spin-orbit effects) the DFT density of states, and the factor of m^*/m_0 arises from mass renormalization beyond the scope of DFT. Writing S in the random-phase approximation (RPA) [39] guides our expectations for its evolution under strained conditions,

$$S_{\mathrm{RPA}} = \frac{1}{1 - IN(E_F)}, \tag{4}$$

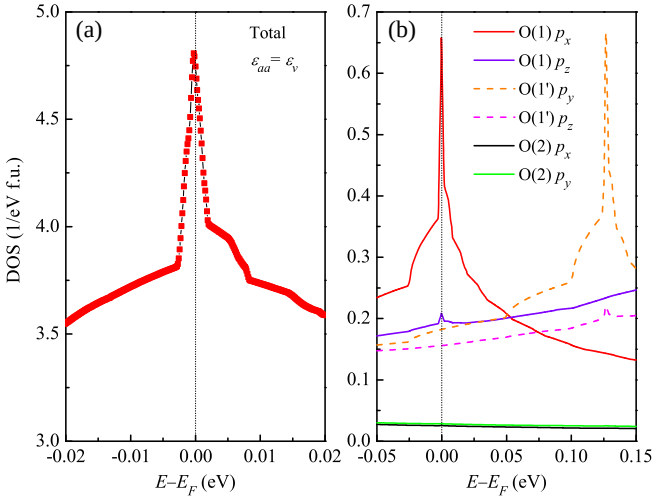

FIG. 5. (a) Calculated DOS at the critical strain, at which the calculated van Hove singularity is located exactly at the Fermi level. Note the very small width (3 meV) and weight (0.0015 e^- per spin channel) of the peak in the DOS. (b) Partial DOS projected onto different O orbitals. The orbitals that are not shown have negligible weight.

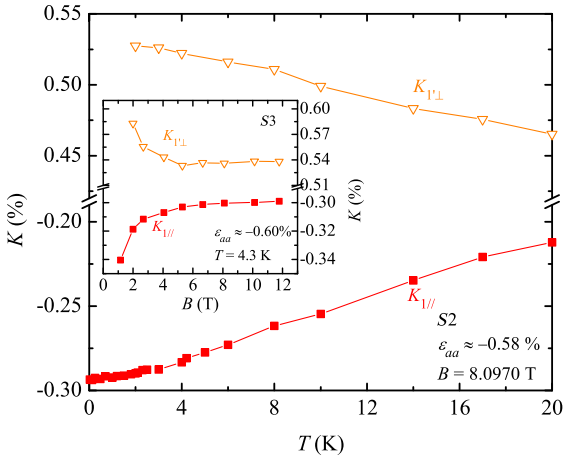

FIG. 6. Main panel: Temperature dependence of $K_{1\|}$ and $K_{1'\perp}$ evaluated at the critical strain ε_v, $B = 8.0970$ T, and $\mathbf{B}\|\mathbf{b}$. Inset: Field dependence of $K_{1\|}$ and $K_{1'\perp}$ measured at ε_v and 4.3 K.

where $N(E_F)$ is the actual DOS. Then, the total uniform magnetic field is the sum of the external field and the induced response, the latter being enhanced compared to the noninteracting case by the factor S. Note that the orbital moment $\mathbf{L}$ in Eq. (1) is assumed to be generated by the spin magnetization through spin-orbit coupling. In addition, there is another orbital term (paramagnetic van Vleck), which is not enhanced in the same way as χ_s. While usually considered small [29], an accurate accounting is not expected in the DFT framework. As indicated by Eqs. (3) and (4), the strain-dependent enhancement of S is important as a mechanism for transferring anomalous responses (linked to the VHS) to orbitals other than Ru d_{xy} and the corresponding hybridizing Op. Notable also is that, in principle, S can be more sensitive to the enhancement of the DOS than χ_s itself. To establish relevance, consider that inelastic neutron-scattering measurements indicate χ_s is enhanced by about a factor of 7 compared to the DFT DOS, viz., $[\chi_s(\varepsilon_{aa}=0)/\chi_{s0}^{\mathrm{DFT}}(\varepsilon_{aa}=0)] \sim 7$ [24], with the enhancement originating from a mass renormalization factor ($m^*/m_0 \sim 3.5$ [3]), and an inferred Stoner factor ($S \sim 2$). Using Eq. (4), $IN(E_F) \approx 0.5$ at zero strain, and with $N(E_F)$ increased by 30%, as in Fig. 5(a), leads to an inferred increase of S from 2 to 3. Thus, if m^*/m_0 and I are taken as strain independent, one gets $[\chi_s(\varepsilon_{aa}=\varepsilon_v)/\chi_{s0}^{\mathrm{DFT}}(\varepsilon_{aa}=\varepsilon_v)] \sim 10.5$, $[\chi_s(\varepsilon_{aa}=\varepsilon_v)/\chi_{s0}^{\mathrm{DFT}}(\varepsilon_{aa}=0)] \sim 14$, and thus $[\chi_s(\varepsilon_{aa}=\varepsilon_v)/\chi_s(\varepsilon_{aa}=0)] \sim 2$, namely, a factor of 2 enhancement in actual spin susceptibility at the critical strain relative to zero strain.

Symmetry considerations indicate that only O(1) p_x orbitals couple with Ru d_{xy} states at Y, and therefore, only the O(1) p_x orbitals are expected to be directly sensitive to the VHS [see Fig. 5(b)]. Thus, one might infer that only the O(1) Knight shift should be affected by the DOS peak at the VHS. However, on general grounds, all sites are sensitive because of the increased Stoner enhancement factor S. Indeed, all measured Knight shifts are affected by strain (Fig. 4), with $K_{1\|}$ more so, presumably because of the direct influence of increased γ band DOS. The strain-induced reduction of the Korringa ratio [40,41] shown in the inset of Fig. S5(a) of the Supplemental Material [32] for the case $\mathbf{B}\|\mathbf{b}$, is consistent with an enhanced Stoner factor S.

Experimental evidence for the narrow VHS and its influences on physical properties is shown in Fig. 6, which depicts shifts with strikingly strong field and temperature dependences for $\varepsilon_{aa} = \varepsilon_v$. The observations are qualitatively consistent with comparable energy scales for Zeeman, thermal, and VHS terms, where, for instance, the broadening of the Fermi distribution progressively weakens the sensitivity of thermodynamic properties to the VHS even when it is situated precisely at the chemical potential [42]. Similar observations for the magnetization were previously reported in a doping study in which the effects of substitution of La for Sr in $Sr_{2-y}La_yRuO_4$ were interpreted as evidence for moving γ-band Fermi energy to the X and Y points of the Brillouin zone [43]. These behaviors are even more striking when compared to expectations in a single-particle framework because the Zeeman coupling shifts the VHS singularity away from the chemical potential. The saturating temperature dependence at fixed field strength that follows is at odds with observations and warrants further study in the context of quantum critical behavior which can be boosted by Stoner enhancement (see below).

For a semiquantitative evaluation of the Stoner enhancement and the subsequent impact on the observable quantities, the data are compared to the results of the DFT calculations. As stated, the inherent deficiency of the DFT

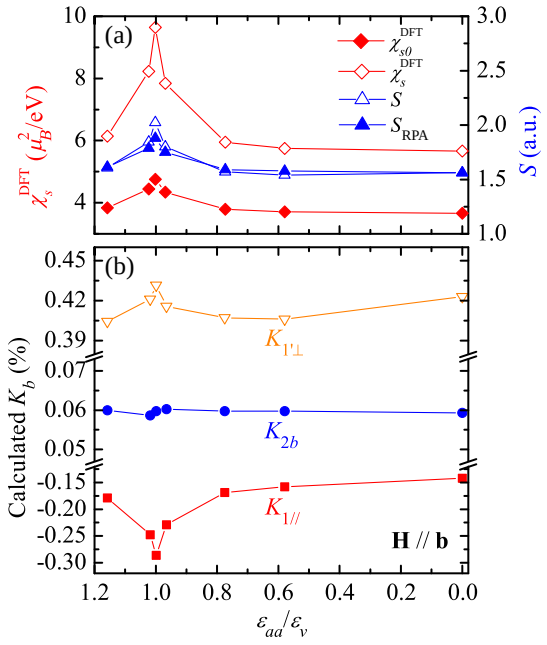

FIG. 7. (a) Calculated magnetic susceptibility in DFT. $\chi_{s0}^{\mathrm{DFT}} \equiv \mu_B^2 N(E_F)$ is the noninteracting susceptibility, χ_s^{DFT} is obtained by dividing the calculated magnetization by the applied field, $M_s/\mu_B H$. The average DFT Stoner factor $S = \chi_s^{\mathrm{DFT}}/\chi_{s0}^{\mathrm{DFT}}$ and $S_{\mathrm{RPA}} = 1/[1 - IN(E_F)]$. Here, S_{RPA} is normalized to S obtained from the calculated DFT result at zero strain. Its variation with strain is calculated from Eq. (4) and the strain-dependent DFT density of states. (b) Calculated total Knight shifts for $\mathbf{H}\|\mathbf{b}$ for the three sites, O(1), O(1′), and O(2), as a function of normalized strain. See the text for details.

calculations for such a strongly correlated material as Sr_2RuO_4 forces deviations from the usual procedure. The standard calculations, such as those presented in Ref. [26], are unstable against spontaneous formation of a ferromagnetic state. The tendency toward this instability is reduced somewhat arbitrarily by scaling the Hund's coupling by half. This ensures numerically stable calculations in external fields up to at least 5 T, even at $\varepsilon_{aa} = \varepsilon_v$. The impact of the reduced Hund's coupling appears to produce systematic errors in related absolute parameters but less so for the relative changes induced by strain. For example, for the selected scaling, Fig. 7(a) indicates that the calculated $\chi_s^{\mathrm{DFT}}(\varepsilon_{aa} = 0)$ renormalization is approximately 1.6, whereas the known correlation-induced mass enhancement is about 3.5 [3]. Therefore, the downscaling is too strong. Given this caveat, at the critical strain, $\chi_s^{\mathrm{DFT}}(\varepsilon_{aa} = \varepsilon_v)$ is enhanced over $\chi_s^{\mathrm{DFT}}(\varepsilon_{aa} = 0)$ by about 70%, while $S(\varepsilon_v)$ itself is enhanced by a much smaller factor, about 30% over $S(0)$ [right frame of Fig. 7(a)]. The scaling for the shifts should follow approximately these factors. Namely, the enhancement of $K_{1\|}$ is expected to scale with χ_s, and therefore, of order 70%, whereas the enhancement of $K_{1'\perp}$ being sensitive to enhancement of S is expected to be much smaller, of order 30%. The former enhancement matches the data in Fig. 4 well, as well as the calculations presented in Fig. 7. The latter enhancement of 30% is relatively larger than the experimental results [Fig. 4(a)], as well as the calculations [Fig. 7(b)], which are both $\simeq$10%. The discrepancy could be associated with unaccounted-for nonsingular contributions, such as in an orbital part (van Vleck or induced through spin-orbit coupling), or nonlinearities, as documented in Fig. 6.

Therefore, the qualitative conclusions from the experiments and in comparing to the DFT calculations are as follows: (1) There are two mechanisms for enhancing the Knight shifts near the critical strain, one applicable to all sites and field directions and the other only to $K_{1\|}$. Both are directly related to the DOS enhancement and show unambiguously that the maximum in T_c indeed coincides with that in DOS. (2) Ferromagnetic spin fluctuations intensify substantially at the same strain due to Stoner enhancement. This effect may also play a key role in boosting T_c. (3) The nonlinear magnetic response for $\varepsilon_{aa} \simeq \varepsilon_v$ and at low temperatures and magnetic fields appears to deviate from the expected single-particle response and are offered here as evidence for both the enhancement of the spin fluctuations, as well as the proximity to a ferromagnetic instability.

Expanding further on point (3) above, the strain-dependent enhancement of S provides a natural explanation to the recently reported resistivity measurements on stressed samples [27] in which deviations from standard Fermi-liquid behavior were observed and interpreted in terms of the DOS singularity [44]. In fact, the behavior may also be connected to the enhanced Stoner factor near the critical strain. Reported was the existence of a crossover temperature T^*, at which the electrical resistivity $\rho = \rho_0 + AT^\delta$ changes from the Fermi-liquid behavior $\delta = 2$ to approximately 1.5–1.6. Note that this behavior is close to what is expected for ferromagnetic spin-fluctuation behavior ($\delta \sim 4/3$–$5/3$) [45]. Moreover, $T^* \propto S^{-1}$ varies strongly with strain [see Fig. S1(b) in the Supplemental Material [32]] and is minimized at ε_v. Both this observation and the nonlinearities in the shifts (Fig. 6) indicate S peaks at ε_v.

Finally, some comments on the data collected for field aligned parallel the **c** axis are in order. In principle, one would expect similar behavior to that for the in-plane field; however, it appears that K_c behaves in a way difficult to rationalize in total. For strain $\varepsilon_{aa} \leq -0.63\%$, a single absorption peak at approximately 0.29% shift is observed for $O(1, 1')$ with only a small increase in the range of ε_v. For larger strain $\varepsilon_{aa} = -0.72\%$, the peak broadens considerably and could be construed as exhibiting two components but with drastically reduced first moment. The drop in intensity is likely a T_1 effect, a consequence of a (relatively) rapid pulse repetition rate [see Fig. S5(b) in the Supplemental Material [32]]. The apparent spectral line "splitting" and distorted line shape are consistent with what could result from a strain gradient along with a nonlinear variation of shift with strain. The main challenge, however,

is to explain the observed evolution on approaching ε_v from smaller strain, where the DFT calculations indicate larger shifts for O(1) than for $O(1')$.

It is possible that the orbital contributions play a more important role for this field orientation ($\mathbf{B}\|\mathbf{c}$). Interestingly, for the orbital part of K_{1c}, and to some extent, of $K_{1'c}$, the calculations predict a sizeable enhancement, suggesting that the van Vleck contribution is not dominant, or, at least, less prominent here than for the in-plane fields, and, conversely, the SOC induces sizeable orbital Knight shifts. Moreover, the sign of this orbital contribution is the opposite of the spin shifts, so there is a tendency toward cancellation. It is believed that correlation effects enhance the SOC in Sr_2RuO_4 by about a factor of 2 [46]. Empirically, if the O(1) and $O(1')$ shifts are assumed to be entirely generated by SOC, while the O(2) shift is entirely van Vleck, a reasonable agreement with experiment is obtained but with small but not negligible peak splittings for strains near ε_v (Fig. S6 in the Supplemental Material [32]). Clearly, the NMR spectra for the field parallel to **c** require further investigations.

IV. CONCLUSION

We demonstrate by means of the NMR spectroscopy under uniaxial stress and corresponding density-functional calculations that there are *two* different effects associated with the strain-induced VHS, which both need to be taken into account, namely, the enhancement of the DOS associated with the γ-band Fermi energy passing through the VHS at the Y point of the Brillouin zone, and a substantial Stoner enhancement S. Associated with the enhanced S is an intensification of ferromagnetic spin fluctuations and strong nonlinearities in the spin susceptibility to the lowest temperatures studied. This finding has immediate ramifications for superconductivity. Namely, first, the DOS is enhanced near the VHS point. In the first approximation, this effect strongly favors some singlet pairings, such as extended s, $d_{zx} \pm id_{yz}$, or $d_{x^2-y^2}$ mildly favors the d_{xy} pairing and less so any triplet pairing. However, this enhancement of the DOS through the Stoner factor boosts ferromagnetic spin fluctuations, which favors triplet states and seems to *disfavor* singlet pairing. Experimentally and theoretically, these two effects are comparable, and therefore, it is unclear which is stronger. More information will be gained by studying NMR in the superconducting state as a function of strain.

ACKNOWLEDGMENTS

We thank S. A. Kivelson, S. Raghu, J. D. Thompson, and F. Zhang for insightful discussions and J. D. Thompson for magnetic properties characterization. This work was supported in part by the Laboratory Directed Research and Development (LDRD) program of Los Alamos National Laboratory under Project No. 20170204ER. Y. L. acknowledges partial support through the LDRD and 1000 Youth Talents Plan of China. N. K. acknowledges the support from JSPS KAKNHI (Grant No. 18K04715). I. I. M. is supported by ONR through the NRL basic research program. This work is supported in part by the National Science Foundation (Grants No. DMR-1410343 and No. DMR-1709304).

APPENDIX: FURTHER CONSIDERATION REGARDING STONER RENORMALIZATION

The experiments and calculations clearly demonstrate the importance of Stoner renormalization near the critical strain, but this is evaluated only semiquantitatively. For example, the RPA-like Eq. (4) implies a uniform renormalization of the exchange splitting over the entire Fermi surface. In actual calculations, this splitting varies substantially over the Fermi surface (depicted in Fig. 8). Still, it remains a qualitatively reasonable approximation. In Fig. 7, we show the results of direct calculations of spin susceptibility inferred by calculating the induced magnetization $M_{s0}(H)$ resulting from a small applied field. The full DFT susceptibility shown in Fig. 7 is $M_s(H)/H$, and the Stoner factor $S = M_s(H)/M_{s0}(H)$, with $M_{s0}(H) = \mu_B^2 N(E_F)H$ the Pauli result for noninteracting electrons.

Figure 8 indicates that the exchange splitting for the same external field is larger for the α and β bands than for the γ band and that this disparity is about twice larger at the critical strain than for the unstrained structure. Overall, in the in the α and β bands, the local Stoner factor (the enhancement of the exchange splitting of the electronic states) varies between 3.2 and 4.7 , and in the γ band it is between 5.7 and 10.0, about a factor of 2 larger than for the unstrained structure. Consequently, it is entirely possible that this variation will weight differently the dipole and the spin-contact contributions. This is consistent with the fact that the temperature dependence of the in-plane and only in-plane Knight shifts are opposite that of the uniform susceptibility at $T \lesssim 100$ K, and only these shifts are affected by the VHS in our experiment [29].

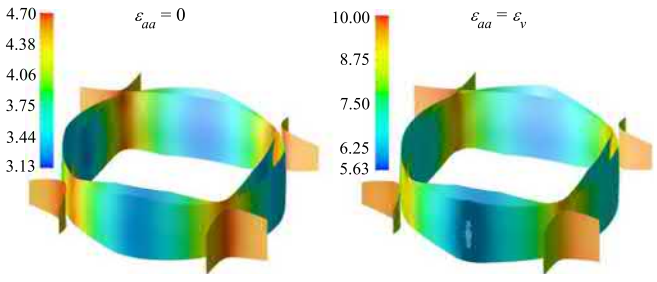

FIG. 8. Calculated Fermi surfaces (nonrelativistic) with no orthorhombic strain (left) and the strain corresponding to the VHS (right). No additional scaling of the Stoner interaction is applied, as opposed to the Knight-shift calculation (Fig. 7 and main text). The surfaces are colored with the calculated exchange splitting in a small uniform external field H normalized to $\mu_B H = 1.6$ meV. Note the different color scales for the two panels.

[1] Y. Maeno, H. Hashimoto, K. Yoshida, S. Nishizaki, T. Fujita, J. G. Bednorz, and F. Lichtenberg, *Superconductivity in a Layered Perovskite without Copper*, Nature (London) **372**, 532 (1994).

[2] T. Rice and M. Sigrist, Sr_2RuO_4*: An Electronic Analogue of* ^{3}He*?*, J. Phys. Condens. Matter **7**, L643 (1995).

[3] A. P. Mackenzie and Y. Maeno, *The Superconductivity of* Sr_2RuO_4 *and the Physics of Spin-Triplet Pairing*, Rev. Mod. Phys. **75**, 657 (2003).

[4] Y. Maeno, S. Kittaka, T. Nomura, S. Yonezawa, and K. Ishida, *Evaluation of Spin-Triplet Superconductivity in* Sr_2RuO_4, J. Phys. Soc. Jpn. **81**, 011009 (2012).

[5] C. Kallin, *Chiral p-Wave Order in* Sr_2RuO_4, Rep. Prog. Phys. **75**, 042501 (2012).

[6] A. P. Mackenzie, T. Scaffidi, C. W. Hicks, and Y. Maeno, *Even Odder after Twenty-Three Years: The Superconducting Order Parameter Puzzle of* Sr_2RuO_4, npj Quantum Mater. **2**, 40 (2017).

[7] G. M. Luke, Y. Fudamoto, K. M. Kojima, M. I. Larkin, J. Merrin, B. Nachumi, Y. J. Uemura, Y. Maeno, Z. Q. Mao, Y. Mori *et al.*, *Time-Reversal Symmetry-Breaking Superconductivity in* Sr_2RuO_4, Nature (London) **394**, 558 (1998).

[8] J. Xia, Y. Maeno, P. T. Beyersdorf, M. M. Fejer, and A. Kapitulnik, *High Resolution Polar Kerr Effect Measurements of* Sr_2RuO_4*: Evidence for Broken Time-Reversal Symmetry in the Superconducting State*, Phys. Rev. Lett. **97**, 167002 (2006).

[9] K. Ishida, H. Mukuda, Y. Kitaoka, K. Asayama, Z. Q. Mao, Y. Mori, and Y. Maeno, *Spin-Triplet Superconductivity in* Sr_2RuO_4 *Identified by* ^{17}O *Knight Shift*, Nature (London) **396**, 658 (1998).

[10] H. Murakawa, K. Ishida, K. Kitagawa, Z. Q. Mao, and Y. Maeno, *Measurement of the* ^{101}Ru*-Knight Shift of Superconducting* Sr_2RuO_4 *in a Parallel Magnetic Field*, Phys. Rev. Lett. **93**, 167004 (2004).

[11] J. A. Duffy, S. M. Hayden, Y. Maeno, Z. Mao, J. Kulda, and G. J. McIntyre, *Polarized-Neutron Scattering Study of the Cooper-Pair Moment in* Sr_2RuO_4, Phys. Rev. Lett. **85**, 5412 (2000).

[12] J. R. Kirtley, C. Kallin, C. W. Hicks, E.-A. Kim, Y. Liu, K. A. Moler, Y. Maeno, and K. D. Nelson, *Upper Limit on Spontaneous Supercurrents in* Sr_2RuO_4, Phys. Rev. B **76**, 014526 (2007).

[13] C. W. Hicks, J. R. Kirtley, T. M. Lippman, N. C. Koshnick, M. E. Huber, Y. Maeno, W. M. Yuhasz, M. B. Maple, and K. A. Moler, *Limits on Superconductivity-Related Magnetization* Sr_2RuO_4 *and* $PrOs_4Sb_{12}$ *from Scanning SQUID Microscopy*, Phys. Rev. B **81**, 214501 (2010).

[14] S. Yonezawa, T. Kajikawa, and Y. Maeno, *First-Order Superconducting Transition of* Sr_2RuO_4, Phys. Rev. Lett. **110**, 077003 (2013).

[15] E. Hassinger, P. Bourgeois-Hope, H. Taniguchi, S. R. de Cotret, G. Grissonnanche, M. S. Anwar, Y. Maeno, N. Doiron-Leyraud, and L. Taillefer, *Vertical Line Nodes in the Superconducting Gap Structure of* Sr_2RuO_4, Phys. Rev. X **7**, 011032 (2017).

[16] S. Kittaka, S. Nakamura, T. Sakakibara, N. Kikugawa, T. Terashima, S. Uji, D. A. Sokolov, A. P. Mackenzie, K. Irie, Y. Tsutsumi *et al.*, *Searching for Gap Zeros in* Sr_2RuO_4 *via Field-Angle-Dependent Specific-Heat Measurement*, J. Phys. Soc. Jpn. **87**, 093703 (2018).

[17] B. Kim, S. Khmelevskyi, I. I. Mazin, D. F. Agterberg, and C. Franchini, *Anisotropy of Magnetic Interactions and Symmetry of the Order Parameter in Unconventional Superconductor* Sr_2RuO_4, npj Quantum Mater. **2**, 37 (2017).

[18] J. Mravlje, M. Aichhorn, T. Miyake, K. Haule, G. Kotliar, and A. Georges, *Coherence-Incoherence Crossover and the Mass-Renormalization Puzzles in* Sr_2RuO_4, Phys. Rev. Lett. **106**, 096401 (2011).

[19] L. de' Medici, J. Mravlje, and A. Georges, *Janus-Faced Influence of Hund's Rule Coupling in Strongly Correlated Materials*, Phys. Rev. Lett. **107**, 256401 (2011).

[20] A. Georges, L. de' Medici, and J. Mravlje, *Strong Correlations from Hund's Coupling*, Annu. Rev. Condens. Matter Phys. **4**, 137 (2013).

[21] I. I. Mazin and D. J. Singh, *Electronic Structure and Magnetism in Ru-Based Perovskites*, Phys. Rev. B **56**, 2556 (1997).

[22] Y. Sidis, M. Braden, P. Bourges, B. Hennion, S. NishiZaki, Y. Maeno, and Y. Mori, *Evidence for Incommensurate Spin Fluctuations in* Sr_2RuO_4, Phys. Rev. Lett. **83**, 3320 (1999).

[23] I. I. Mazin and D. J. Singh, *Competitions in Layered Ruthenates: Ferromagnetism versus Antiferromagnetism and Triplet versus Singlet Pairing*, Phys. Rev. Lett. **82**, 4324 (1999).

[24] P. Steffens, Y. Sidis, J. Kulda, Z. Q. Mao, Y. Maeno, I. Mazin, and M. Braden, *Spin Fluctuations in* Sr_2RuO_4 *from Polarized Neutron Scattering: Implications for Superconductivity*, Phys. Rev. Lett. **122**, 047004 (2019).

[25] A. Damascelli, D. H. Lu, K. M. Shen, N. P. Armitage, F. Ronning, D. L. Feng, C. Kim, Z.-X. Shen, T. Kimura, Y. Tokura *et al.*, *Fermi Surface, Surface States, and Surface Reconstruction in* Sr_2RuO_4, Phys. Rev. Lett. **85**, 5194 (2000).

[26] A. Steppke, L. Zhao, M. E. Barber, T. Scaffidi, F. Jerzembeck, H. Rosner, A. S. Gibbs, Y. Maeno, S. H. Simon, A. P. Mackenzie *et al.*, *Strong Peak in* T_c *of* Sr_2RuO_4 *under Uniaxial Pressure*, Science **355**, eaaf9398 (2017).

[27] M. E. Barber, A. S. Gibbs, Y. Maeno, A. P. Mackenzie, and C. W. Hicks, *Resistivity in the Vicinity of a van Hove Singularity:* Sr_2RuO_4 *under Uniaxial Pressure*, Phys. Rev. Lett. **120**, 076602 (2018).

[28] S. Kivelson (private communication).

[29] T. Imai, A. W. Hunt, K. R. Thurber, and F. C. Chou, ^{17}O *NMR Evidence for Orbital Dependent Ferromagnetic Correlations in* Sr_2RuO_4, Phys. Rev. Lett. **81**, 3006 (1998).

[30] R. K. Harris, E. D. Becker, S. M. C. de Menezes, R. Goodfellow, and P. Granger, *NMR Nomenclature. Nuclear Spin Properties and Conventions for Chemical Shifts (IUPAC Recommendations 2001)*, Pure Appl. Chem. **73**, 1795 (2001).

[31] A postanneal in air at reduced temperatures (approximately 450 °C) leads to smaller-than-expected absorption from the apical O(2) sites, indicating that the ^{17}O substitution to the O(1) sites likely proceeds through the apical sites.

[32] See Supplemental Material at http://link.aps.org/supplemental/10.1103/PhysRevX.9.021044 for experimental setup, sample characterization, field-swept spectra,

spin-lattice relaxation rate, and electric field gradient (EFG) results of Sr_2RuO_4 under uniaxial stress, as well as additional theoretical details.

[33] The clamping structure is not perfectly rigid, and as a consequence, the actual sample compression is smaller than what is measured by the dilatometer [34].

[34] C. W. Hicks, M. E. Barber, S. D. Edkins, D. O. Brodsky, and A. P. Mackenzie, *Piezoelectric-Based Apparatus for Strain Tuning*, Rev. Sci. Instrum. **85**, 065003 (2014).

[35] P. Blaha, K. Schwarz, G. Madsen, D. Kvasnicka, and J. Luitz, *WIEN2K, An augmented Plane Wave+Local Orbitals Program for Calculating Crystal Properties*, Technische Universität Wien, Austria, 2001.

[36] H. Mukuda, K. Ishida, Y. Kitaoka, K. Asayama, Z. Mao, Y. Mori, and Y. Maeno, *Novel Character of Spin Fluctuations in Spin-Triplet Superconductor* Sr_2RuO_4 ^{17}O*-NMR Study*, J. Phys. Soc. Jpn. **67**, 3945 (1998).

[37] E. Pavarini and I. I. Mazin, *First-Principles Study of Spin-Orbit Effects and NMR in* Sr_2RuO_4, Phys. Rev. B **74**, 035115 (2006).

[38] M. W. Haverkort, I. S. Elfimov, L. H. Tjeng, G. A. Sawatzky, and A. Damascelli, *Strong Spin-Orbit Coupling Effects on the Fermi Surface of* Sr_2RuO_4 *and* Sr_2RhO_4, Phys. Rev. Lett. **101**, 026406 (2008).

[39] In principle, the polarization operators and the Stoner factors in this formula are matrices in the band indices and reciprocal lattice vectors. In the discussion here, we neglect these complexities.

[40] J. Korringa, *Nuclear Magnetic Relaxation and Resonance Line Shift in Metals*, Physica (Amsterdam) **16**, 601 (1950).

[41] M. Hirata, K. Ishikawa, K. Miyagawa, K. Kanoda, and M. Tamura, ^{13}C *NMR Study on the Charge-Disproportionated Conducting State in the Quasi-Two-Dimensional Organic Conductor* α-$(BEDT\text{-}TTF)_2I_3$, Phys. Rev. B **84**, 125133 (2011).

[42] R. Nourafkan and S. Acheche, *Temperature Dependence of the NMR Knight Shift in Pnictides: Proximity to a van Hove Singularity*, Phys. Rev. B **98**, 161116(R) (2018).

[43] N. Kikugawa, C. Bergemann, A. P. Mackenzie, and Y. Maeno, *Band-Selective Modification of the Magnetic Fluctuations in* Sr_2RuO_4*: A Study of Substitution Effects*, Phys. Rev. B **70**, 134520 (2004).

[44] R. Hlubina, *Effect of Impurities on the Transport Properties in the van Hove Scenario*, Phys. Rev. B **53**, 11344 (1996).

[45] G. R. Stewart, *Non-Fermi-Liquid Behavior in d- and f-Electron Metals*, Rev. Mod. Phys. **73**, 797 (2001).

[46] M. Kim, J. Mravlje, M. Ferrero, O. Parcollet, and A. Georges, *Spin-Orbit Coupling and Electronic Correlations in* Sr_2RuO_4, Phys. Rev. Lett. **120**, 126401 (2018).

Supplemental Material:

Normal state ^{17}O NMR studies of Sr_2RuO_4 under uniaxial stress

Yongkang Luo[1,2*], A. Pustogow[1], P. Guzman[1], A. P. Dioguardi[3], S. M. Thomas[3], F. Ronning[3], N. Kikugawa[4], D. A. Sokolov[5], F. Jerzembeck[5], A. P. Mackenzie[5,6], C. W. Hicks[5], E. D. Bauer[3], I. I. Mazin[7], and S. E. Brown[1†]

[1] *Department of Physics and Astronomy, University of California, Los Angeles, CA 90095, USA;*
[2] *Wuhan National High Magnetic Field Center and School of Physics, Huazhong University of Science and Technology, Wuhan 430074, China;* [3] *Los Alamos National Laboratory, Los Alamos, New Mexico 87545, USA;*
[4] *National Institute for Materials Science, Tsukuba 305-0003, Japan;*
[5] *Max Planck Institute for Chemical Physics of Solids, Dresden 01187, Germany;*
[6] *Scottish Universities Physics Alliance, School of Physics and Astronomy, University of St Andrews, North Haugh, St Andrews KY16 9SS, UK; and*
[7] *Code 6393, Naval Research Laboratory, Washington, DC 20375, USA.*

In this **Supplemental Material (SM)**, we provide the experimental setup, sample characterization, field-swept spectra, spin-lattice relaxation rate and electric field gradient (EFG) results of Sr_2RuO_4 under uniaxial stress, as well as additional theoretical details that further support the discussions in the main text.

SM I: Sample characterizations

Figure S1a is a photograph of the set-up for our NMR measurements under strain. The compressive uniaxial pressure is generated by a set of piezoelectric actuators[1]. A Sr_2RuO_4 sample is glued between two pairs of titanium plates with stycast 2850 (black). To get the best filling factor, a small NMR coil (about 25 turns) is made *in-situ* surrounding the sample after the stycast hardens with 25 μm Cu wire.

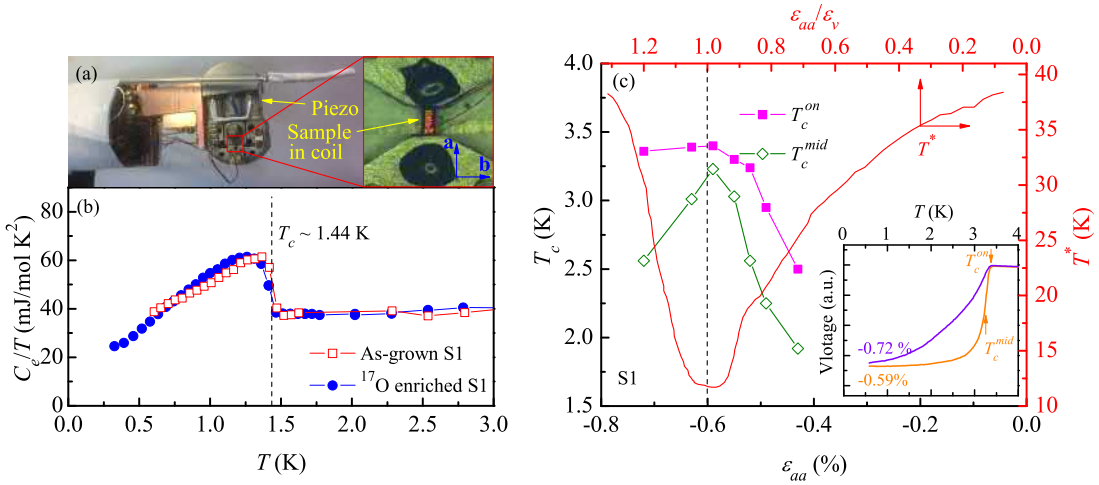

FIG. S1. (a) A photograph of the uniaxial stress apparatus. The stress/strain effect is applied through a set of piezoelectric actuators. The forces are applied uniaxially, and the strain response is measured using a capacitive dilatometer. A small coil is made *in-situ* surrounding the sample that is bonded between two pairs of titanium plates. (b) Electronic specific heat divided by temperature of the Sr_2RuO_4 samples before and after ^{17}O enrichment. Superconducting transitions are clearly visible at about 1.44 K. (c) Strain dependence of superconducting transition from ac magnetization measurements, with critical temperatures T_c^{on} and T_c^{mid} defined in the inset. Maximal T_c is realized near the strain ε_{aa}=−0.6%. The top-right frame displays the profile of T^* reproduced from Ref. [2]. The strains from the respective experiments are aligned using the respective measured maxima in superconducting critical temperature, $T_c(\varepsilon_{aa})$ [3].

The quality of the Sr_2RuO_4 sample measured is characterized by specific heat measurements, as shown in Fig. S1b. The superconducting transitions are clearly visible in C_e/T before and after annealing in ^{17}O atmosphere, with T_c≈1.44 K essentially unaffected. Here C_e is the electronic contribution to specific heat. The jump in C_e/T at the transition as well as the normal state Sommerfeld coefficient are also in good agreement with previous findings[4]. All these measurements guarantee the high quality of the sample studied in this work.

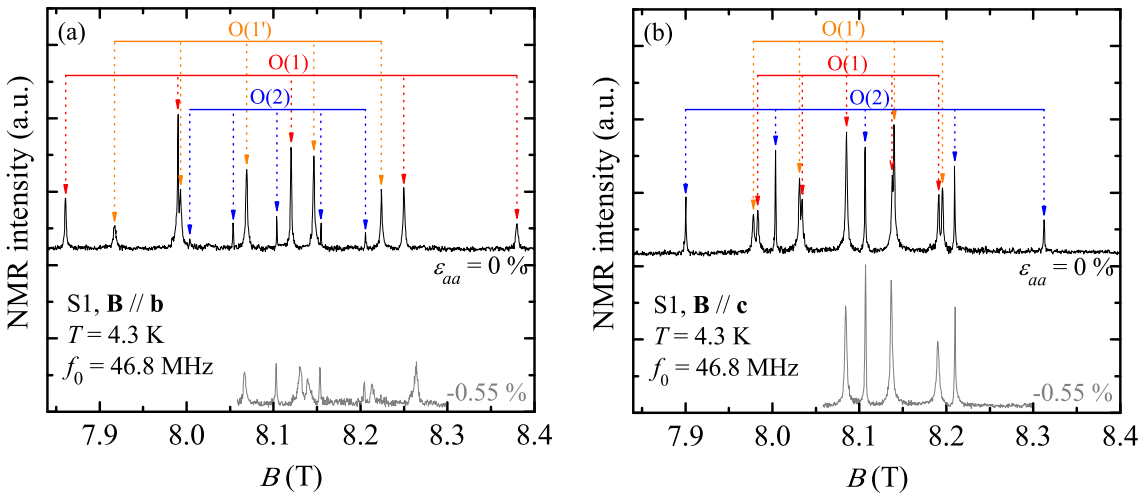

FIG. S2. Comparison of ^{17}O NMR spectra of Sr_2RuO_4 for strain ε_{aa}=0 (black) and −0.55% (grey) where T_c approaches the maximum. (a) measurements with $\mathbf{B}\|\mathbf{b}$, and (b) with $\mathbf{B}\|\mathbf{c}$. At ε_{aa}=0 and $\mathbf{B}\|\mathbf{c}$, the splitting of O(1) and O(1′) satellite peaks is due to a small angular misalignment (∼5°).

In Fig. S2, we present the field-sweep ^{17}O NMR spectra of Sr_2RuO_4 for both $\mathbf{B}\|\mathbf{b}$ (left panel) and $\mathbf{B}\|\mathbf{c}$ (right panel). All the peaks in this field region can be assigned to signals from O(1), O(1′) and O(2) sites, and no extra peaks can be identified. This excludes the impurity phases from other members in $Sr_{n+1}Ru_nO_{3n+1}$ family. For each O site, it shows one central peak ($\frac{1}{2} \leftrightarrow -\frac{1}{2}$) and four satellite peaks corresponding to $\pm\frac{1}{2} \leftrightarrow \pm\frac{3}{2}$ and $\pm\frac{3}{2} \leftrightarrow \pm\frac{5}{2}$, respectively.

TABLE S1. Comparison of Knight shifts and components of the EFG tensor in Sr_2RuO_4 for ε_{aa}=0 (T_c=1.44 K) and −0.55% (T_c=3.3 K). Measurements made at 4.3 K. The asymmetry parameter is calculated by $\eta=(\nu_x-\nu_y)/\nu_z$. The results are from sample S1.

Sites		Quantities	ε_{aa}=0	ε_{aa}=−0.55%	Note
O(1)	K_1	$K_{1\|\|}$ (%)	−0.15(1)	−0.28(2)	
		K_{1c} (%)	+0.29(1)	+0.30(1)	
	EFG(1)	ν_{1a} (MHz)	−0.444(4)	−0.469(7)	ν_{1y}
		ν_{1b} (MHz)	+0.755(5)	+0.778(9)	ν_{1z}=ν_{1Q}
		ν_{1c} (MHz)	−0.311(3)	−0.309(5)	ν_{1x}
	Asymmetry	η_1	0.175(3)	0.206(5)	
O(1′)	$K_{1'}$	$K_{1'\perp}$ (%)	+0.48(1)	+0.52(2)	
		$K_{1'c}$ (%)	+0.29(1)	+0.30(1)	
	EFG(1′)	$\nu_{1'a}$ (MHz)	+0.759(6)	+0.730(9)	$\nu_{1'z}$=$\nu_{1'Q}$
		$\nu_{1'b}$ (MHz)	−0.445(4)	−0.425(6)	$\nu_{1'y}$
		$\nu_{1'c}$ (MHz)	−0.314(4)	−0.305(5)	$\nu_{1'x}$
	Asymmetry	$\eta_{1'}$	0.172(3)	0.164(5)	
O(2)	K_2	K_{2b} (%)	+0.055(6)	+0.066(9)	
		K_{2c} (%)	+0.021(5)	+0.015(3)	
	EFG(2)	ν_{2a} (MHz)	−0.300(2)	−0.303(3)	ν_{2y}
		ν_{2b} (MHz)	−0.300(2)	−0.299(3)	ν_{2x}
		ν_{2c} (MHz)	+0.600(3)	+0.602(4)	ν_{2z}=ν_{2Q}
	Asymmetry	η_2	0.000(1)	0.007(2)	

These satellite peaks arise from nuclear quadrupole interaction with the electric field gradient (EFG) at the nuclear

site, as described by

$$H_Q = \frac{eQV_{zz}}{4I(2I-1)}[3\hat{I_z}^2 - \hat{\mathbf{I}}^2 + \eta(\hat{I_x}^2 - \hat{I_y}^2)], \tag{S1}$$

where $\hat{\mathbf{I}}=(\hat{I_x},\hat{I_y},\hat{I_z})$ is nuclear spin operator, Q is nuclear quadrupole moment, and $\eta=(V_{xx}-V_{yy})/V_{zz}$ is the asymmetry parameter with V_{xx}, V_{yy} and V_{zz} being the components of the EFG tensor. Here we adopt the convention $V_{zz}\geq V_{xx}\geq V_{yy}$, and $V_{xx}+V_{yy}+V_{zz}=0$. In Sr_2RuO_4, V_{zz} is along Ru-O bonding[5]. This allows us to determine principle-axis nuclear quadrupole resonance (NQR) frequency $\nu_Q=\nu_z$ from the spectra shown in Fig. S2. Note that ν_z is related to V_{zz} by

$$\nu_z = \frac{3eQV_{zz}}{2I(2I-1)h}. \tag{S2}$$

Other components of NQR frequencies conform to the formula:

$$\nu_Q' = \nu_Q[\frac{3\cos^2\theta - 1}{2} + \frac{\eta}{2}\sin^2\theta\cos 2\phi], \tag{S3}$$

where θ and ϕ are respectively polar and azimuthal angles as defined in regular **xyz**-frames, see Fig. S3a. Eq. (S3) also enables us to verify the sample orientation with respect to magnetic field. In fact, for $\mathbf{B}\|\mathbf{c}$ and $\varepsilon_{aa}=0$, we should expect the NQR peaks of O(1) and O(1′) to merge. The splitting of them seen in Fig. S2b is a consequence of small angular misalignment which we estimate to be $\theta\sim5^o$ according to Eq. (S3).

Table S1 summarizes all the physical parameters of O(1), O(1′) and O(2) sites after the correction of angular misalignment. The results at ambient pressure are in good agreement with that reported by Mukuda *et al* [5].

SM II: Strain dependent ν_Q – experimental and theoretical

Under strain, the peaks of O(2) sites remain essentially unchanged, while both O(1) and O(1′) change drastically. In particular, for $\mathbf{B}\|\mathbf{c}$, the satellite peaks of O(1) and O(1′) merge "coincidentally" when $\varepsilon_{aa}=-0.55\%$, implying that the two move at different rates under strain. The strain dependencies of ν_Q and η are displayed in Fig. S3b-c. Evidently, the changes of ν_Q in O(1) and O(1′) are of opposite signs. This is because an expansive strain is induced along **b**-axis, *i.e.* $\varepsilon_{bb}>0$, which is characterized by the Poisson's ratio $-\varepsilon_{bb}/\varepsilon_{aa}=0.40$ for Sr_2RuO_4[6]. We note that the ratio of the slopes in $\nu_{1Q}(\varepsilon_{aa})$ and $\nu_{1'Q}(\varepsilon_{aa})$ is very close to Poisson's ratio.

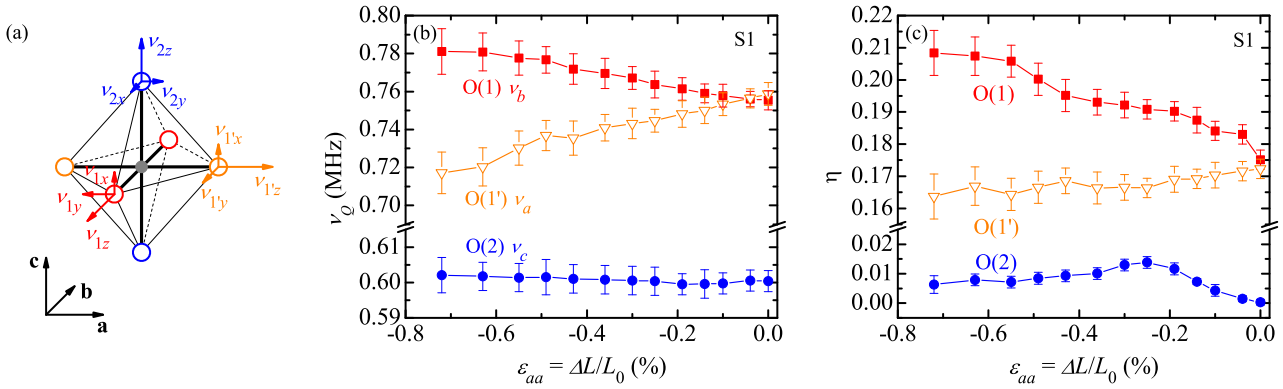

FIG. S3. (a) Schematic sketch of EFG tensors at O sites of Sr_2RuO_4. The principle component ν_z is along the Ru-O bond, and the length of the arrows characterizes the magnitude of ν_i (i=x,y,z). (b) and (c) show strain dependence of $\nu_Q(=\nu_z)$ and asymmetry parameter η, respectively.

Theoretically, ν_Q usually consists of two contributions: point charge (ionic) of other ions and on-site hole in O p orbitals,

$$\nu_Q = \nu_Q^{ionic} + \nu_Q^{hole}, \tag{S4}$$

we shall consider them separately. The ionic term can be calculated by (in SI unit):

$$\nu_Q^{ionic}[\mathrm{Hz}] = \frac{1}{4\pi\epsilon_0}\frac{3eQV_{zz}^{ionic}}{2I(2I-1)h}(1-\gamma_\infty), \tag{S5}$$

where nuclear spin I=5/2, quadruple moment Q=-0.026×10^{-28} m^2, and γ_∞ refers to the Sternheimer antishielding factor which accounts for the contribution from the distortion of the O ion both by the local EFG and by the quadrupolar field of the nucleus[7]. This antishielding factor turns out to be not important in Sr_2RuO_4, much weaker than in cuprates[7], we therefore ignore it hereafter. V_{zz}^{ionic} can be calculated with the crystalline lattice parameters a=b=3.8603 Å, and c=12.729 Å, and coordinates of the ions Sr^{2+} (0.5, 0.5, 0.1468), Ru^{4+} (0, 0, 0), $O(1)^{2-}$ (0.5, 0, 0) and $O(2)^{2-}$ (0, 0, 0.1619)[8].

The on-site hole contribution ν_Q^{hole} is proportional to the hole content (n) in each O orbitals, and the latter can be obtained from DFT calculations by integrating the partial density of states up to Fermi energy, viz.

$$2-n = \int_{-\infty}^{E_F} N(E)dE. \tag{S6}$$

The variation of n for each O orbitals are displayed in Fig. S4.

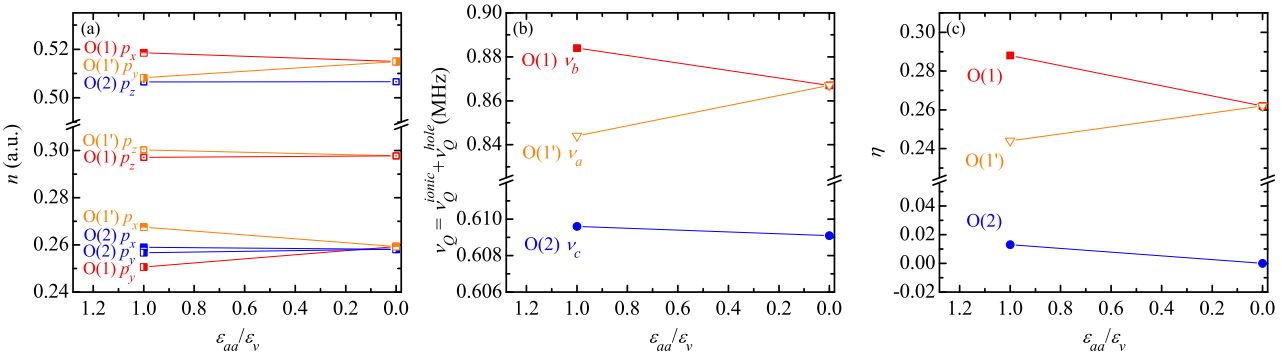

FIG. S4. (a) Comparison of hole content of O orbitals for ε_{aa}=0 and ε_v where the vHS in Sr_2RuO_4 is realized theoretically. (b) and (c) display calculated quadrupolar frequency (ν_Q) and asymmetry parameter (η) as a function of ε_{aa}, respectively.

Taking O(1) p_x orbital as an example, the yielded quadrupoar frequencies are $(\nu_a, \nu_b, \nu_c)_{1,p_x}$=$n_{1,p_x}(q_{xa}, q_{xb}, q_{xc})$, where the ratios q_{xa}=$-2q_{xb}$=$-2q_{xc}$=2.452 MHz for ^{17}O according to previous reports on cuprates[9]. The total quadrupolar frequency should be the sum of the contributions from all the three p orbitals for each O site.

The calculated quadrupolar frequencies ν_Q and the associated asymmetry pramaeter η are shown in Fig. S4b and c, respectively.

Comparison can be made for ν_Q and η between measured (Fig. S3) and calculated (Fig. S4) results. Regardless of some difference in magnitude, agreement between experiment and theory in the evolution trend upon strain effect is striking in both ν_Q and η.

SM III: Spin-lattice relaxation rate

Additional evidence for a vHs comes from the measurements of the spin-lattice relaxation rate $[T_1T]^{-1}$ of Sr_2RuO_4 as shown in Fig. S5b. The $[T_1T]^{-1}$ is recorded for the central transition of the O(1) site and for field $\mathbf{B} \parallel \mathbf{b}$. As a means to extract the strain dependence of the relaxation rate in a minimum of measurement time, the recovery curves at high ($\varepsilon_{aa} = \varepsilon_v$) and low strain ($\varepsilon_{aa} = 0$) were established to follow the appropriate form for spin I=5/2, and dominantly magnetic relaxation governing selective irradiation of the central transition. Between these endpoints, a single recovery was recorded, with short delay time selected prior to application of the echo read sequence, so that the relaxation rate could be inferred from the recorded signal amplitude.

As shown in Fig. S5b, the relaxation is maximum at the strain where the shifts are extremal, consistent with the vHs-tuning scenario. Although only a narrow temperature range is covered, a temperature dependence is clearly

evident in the inset, where the behavior is contrasted to the zero strain results of Ref. [5]. The variation could originate partially or entirely from proximity to the vHs, with the remainder related to correlations. Note that the singularity in two dimensions scales as $\ln(t/T)$, with t the relevant hopping integral, and its effect on thermodynamic properties is rapidly diminished due to thermal broadening of the Fermi function.

In order to investigate the magnetic fluctuations of Sr_2RuO_4, we also consider the Korringa ratio $\alpha \equiv S_K/(K_s^2 T_1 T)$, where $S_K=(\hbar/4\pi k_B)(\gamma_e/\gamma_n)^2$ with $\gamma_e=2.8025\times10^4$ MHz/T being electron gyromagnetic ratio. The standard analysis assumes an *isotropic* hyperfine interaction and a single susceptibility. Then, for the case of uncorrelated electrons, $\alpha=1$ [10]. In the presence of antiferromagnetic correlations, the enhanced $\chi(\mathbf{q})$ around the antiferromagnetic wave vector $\mathbf{q}$ promotes $1/T_1T$ but has little effect on K_s, which renders $\alpha>1$. The situation is opposite for ferromagnetic correlations, that is, $\alpha<1$. A quantitative analysis for *anisotropic* coupling[11], as applies here, requires a more detailed angular-dependent study of both shifts and relaxation rates. Consider, for example, the uncorrelated case, and coupling only to the in-plane $2p_x$ orbital at the O(1) site with $\mathbf{B} \parallel \mathbf{b}$, where the modified $\alpha\approx2.5$ is expected. For Sr_2RuO_4, neutron scattering results indicated antiferromagnetic fluctuations[12] and a broad component at small wavevector[13]. A quantitative interpretation of α is potentially complicated by the multiorbital/multiband nature of Sr_2RuO_4. Nevertheless, a trend consistent with enhancement of ferromagnetic fluctuations appears in the inset to Fig. S5a, where a strong minimum-a reduction of 60%-in α is centered around $\varepsilon_{aa}=\varepsilon_v$, for this orientation of magnetic field.

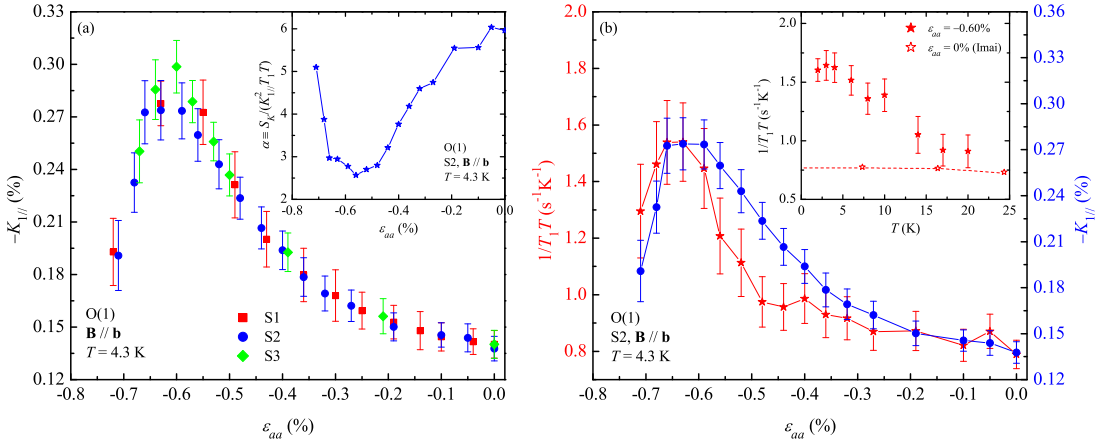

FIG. S5. (a) Strain dependence of $-K_{1\parallel}$ measured from different Sr_2RuO_4 samples. The inset shows the Korringa ratio $\alpha \equiv S/K_{1\parallel}^2 T_1 T$. (b) Magnetization recovery $[T_1T]^{-1}$ of central transition for O(1) site as function of strain ε_{aa}, recorded at T=4.3 K and with magnetic field aligned with **b**-axis. The inset shows a variation with temperature.

SM IV: Comments on the ^{17}O NMR shifts for B ∥ c

In the main text, the NMR Knight shifts of Sr_2RuO_4 for $\mathbf{B} \parallel \mathbf{c}$ were not closely examined. In part, this is because of an apparently reduced sensitivity to the vHs. In particular, for all strains $|\varepsilon_{aa}| < |\varepsilon_v|$, the central transition for the O(1,1′) sites are only weakly changing and remain unresolved, indicating cancellation effects of contributions to the total shifts. Large changes *are* observed for $|\varepsilon_{aa}| > |\varepsilon_v|$, where large drops in spin susceptibility and severe line-broadening are qualitatively consistent with inhomogeneous strain within the measured sample volume and an accompanying amplified sensitivity to the inequivalent environments.

In the DFT calculations for the same quantities, K_{2c} does show essentially full cancellation of the DOS effects, as shown in Fig. S6. On the other hand, both K_{1c} and $K_{1'c}$ appear quite sensitive to the vHs, and, interestingly, in both Fermi and orbital terms. As discussed in the main text, there are two mechanisms by which O electrons can acquire an orbital moment: directly induced by the external field, and via spin-orbit coupling to the induced spin moment. Our calculations show the former effect in K_{1c} and $K_{1'c}$ to be strong, and *opposite in sign to the spin mechanism*. In the raw calculations the amplitude of the orbital shifts is too small to ensure a full cancellation, but,

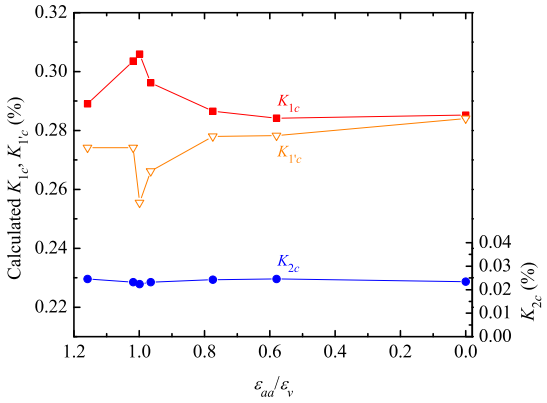

FIG. S6. Calculated total Knight shift of Sr_2RuO_4 for $\mathbf{H} \parallel \mathbf{c}$ for the three sites, O(1), O(1′) and O(2). Some discussion of the disparities between these results and what is observed experimentally is included in the main text.

as discussed in the main text, spin-orbit effects may be considerably enhanced by correlation (Ref. [14]). Assuming a semiphenomenological approach, we plot in Fig. S6 the sum of all contributions to K_{1c} and $K_{1'c}$, *multiplying the orbital part by a factor of four*, without adding any van Vleck constant. The result still show a small split between K_{1c} and $K_{1'c}$ (albeit smaller than the measured peak widths) and an overall good agreement with the measurements. As we stated in the main text, the NMR spectra for the field parallel to **c** require further investigation.

* mpzslyk@gmail.com
† brown@physics.ucla.edu

[1] C. W. Hicks, D. O. Brodsky, E. A. Yelland, A. S. Gibbs, J. A. N. Bruin, M. E. Barber, S. D. Edkins, K. Nishimura, S. Yonezawa, Y. Maeno, et al., *Strong Increase of T_c of Sr_2RuO_4 Under Both Tensile and Compressive Strain*, Science **344**, 283 (2014).
[2] M. E. Barber, A. S. Gibbs, Y. Maeno, A. P. Mackenzie, and C. W. Hicks, *Resistivity in the Vicinity of a van Hove Singularity: Sr_2RuO_4 under Uniaxial Pressure*, Phys. Rev. Lett. **120**, 076602 (2018).
[3] The capacitive reading is an upper bound. In practice, the elasticity of the mounting structure, including the epoxy, leads to reductions. In this article, we have assumed a corrective factor of 0.8, following Ref. [26]. Independent assessment will be evaluated in future benchmark studies.
[4] K. Deguchi, Z. Q. Mao, and Y. Maeno, *Determination of the Superconducting Gap Structure in All Bands of the Spin-Triplet Superconductor Sr_2RuO_4*, J. Phys. Soc. Jpn. **73**, 1313 (2004).
[5] H. Mukuda, K. Ishida, Y. Kitaoka, K. Asayama, Z. Mao, Y. Mori, and Y. Maeno, *Novel Character of Spin Fluctuations in Spin-Triplet Superconductor Sr_2RuO_4 ^{17}O-NMR Study*, J. Phys. Soc. Jpn. **67**, 3945 (1998).
[6] N. Okuda, T. Suzuki, Z. Mao, Y. Maeno, and T. Fujita, *Unconventional Strain Dependence of Superconductivity in Spin-Triplet Superconductor Sr_2RuO_4*, J. Phys. Soc. Jpn. **71**, 1134 (2002).
[7] M. E. Garcia and K. H. Bennemann, *Theoretical study of the structural dependence of nuclear quadrupole frequencies in high-T_c superconductors*, Phys. Rev. B **40**, 8809 (1989).
[8] T. Oguchi, *Electronic band structure of the superconductor Sr_2RuO_4*, Phys. Rev. B **51**, 1385 (1995).
[9] J. Haase, O. P. Sushkov, P. Horsch, and G. V. M. Williams, *Planar Cu and O hole densities in high-T_c cuprates determined with NMR*, Phys. Rev. B **69**, 094504 (2004).
[10] J. Korringa, *Nuclear magnetic relaxation and resonnance line shift in metals*, Physica **16**, 601 (1950).
[11] M. Hirata, K. Ishikawa, K. Miyagawa, K. Kanoda, and M. Tamura, ^{13}C *NMR study on the charge-disproportionated conducting state in the quasi-two-dimensional organic conductor α-(BEDT-TTF)$_2$I$_3$*, Phys. Rev. B **84**, 125133 (2011).
[12] Y. Sidis, M. Braden, P. Bourges, B. Hennion, S. NishiZaki, Y. Maeno, and Y. Mori, *Evidence for Incommensurate Spin Fluctuations in Sr_2RuO_4*, Phys. Rev. Lett. **83**, 3320 (1999).
[13] M. Braden, Y. Sidis, P. Bourges, P. Pfeuty, J. Kulda, Z. Mao, and Y. Maeno, *Inelastic neutron scattering study of magnetic excitations in Sr_2RuO_4*, Phys. Rev. B **66**, 064522 (2002).
[14] M. Kim, J. Mravlje, M. Ferrero, O. Parcollet, and A. Georges, *Spin-Orbit Coupling and Electronic Correlations in Sr_2RuO_4*, Phys. Rev. Lett. **120**, 126401 (2018).